www.nature.com/aps

Acta Pharmacologica Sinica

ARTICLE

Inhibiting von Hippel–Lindau protein-mediated Dishevelled ubiquitination protects against experimental parkinsonism

Jie Shen[1], Qian Zha[1], Qian-hua Yang[1], Yue-qian Zhou[1], Xiao Liang[1], Ying-jie Chen[1], Gui-xia Qi[1], Xiao-jin Zhang[2], Wen-bing Yao[1], Xiang-dong Gao[1] and Song Chen[1]

Dopaminergic neuron degeneration is a hallmark of Parkinson's disease (PD). We previously reported that the inactivation of von Hippel–Lindau (VHL) alleviated dopaminergic neuron degeneration in a *C. elegans* model. In this study, we investigated the specific effects of VHL loss and the underlying mechanisms in mammalian PD models. For in vivo genetic inhibition of VHL, AAV-*Vhl*-shRNA was injected into mouse lateral ventricles. Thirty days later, the mice received MPTP for 5 days to induce PD. Behavioral experiments were conducted on D1, D3, D7, D14 and D21 after the last injection, and the mice were sacrificed on D22. We showed that knockdown of VHL in mice significantly alleviated PD-like syndromes detected in behavioral and biochemical assays. Inhibiting VHL exerted similar protective effects in MPP^+-treated differentiated SH-SY5Y cells and the MPP^+-induced *C. elegans* PD model. We further demonstrated that VHL loss-induced protection against experimental parkinsonism was independent of hypoxia-inducible factor and identified the Dishevelled-2 (DVL-2)/β-catenin axis as the target of VHL, which was evolutionarily conserved in both *C. elegans* and mammals. Inhibiting the function of VHL promoted the stability of β-catenin by reducing the ubiquitination and degradation of DVL-2. Thus, in vivo overexpression of DVL-2, mimicking VHL inactivation, protected against PD. We designed a competing peptide, Tat-DDF-2, to inhibit the interaction between VHL and DVL-2, which exhibited pharmacological potential for protection against PD in vitro and in vivo. We propose the therapeutic potential of targeting the interaction between VHL and DVL-2, which may represent a strategy to alleviate neurodegeneration associated with PD.

Keywords: Parkinson's disease; von Hippel–Lindau; Dishevelled-2; peptide; MPTP; MPP^+

Acta Pharmacologica Sinica (2023) 44:940–953; https://doi.org/10.1038/s41401-022-01014-1

INTRODUCTION

Parkinson's disease (PD) is one of the most common neurodegenerative diseases and is characterized by progressive and selective loss of dopaminergic neurons in the substantia nigra [1]. Based on the rapidly increasing age of the world population, the number of PD patients is expected to double by 2040 compared to 2015 [2]. The main clinical manifestations of PD are motor symptoms, including rest tremor, abnormal posture and pace, muscle rigidity, and bradykinesia, as well as nonmotor symptoms, including hyposmia, constipation, depression, and sleep disorders [3, 4]. The typical pathological feature of PD is the progressive death of dopaminergic neurons in the substantia nigra, which results in a significant reduction in dopamine in the striatum (ST). Lewy bodies also appear in the neurons of PD patients [5, 6]. In recent years, our understanding of PD has significantly increased, but current therapeutic options for PD are limited.

Dopaminergic neurons participate in regulating the response to the environment. The increase in dopamine release can induce locomotor hyperactivity in a new environment [7, 8]. Dopaminergic neurons also play an important role in motor capacity and cognitive ability [9, 10]. The degeneration and apoptosis of dopaminergic neurons contribute to the occurrence and development of PD, and many factors, such as the ecological environment, neuroinflammation, and oxidative stress, are involved in the process. Mitochondrial dysfunction is one of the critical factors contributing to the degeneration and apoptosis of dopaminergic neurons [4, 11]. Mitochondria, the main sites for aerobic respiration in cells, participate in many crucial intracellular activities involved in energy metabolism, signal transduction, and oxidative stress responses [12]. In the mitochondria, complex I serves as an essential part of the mitochondrial respiratory chain. The neurotoxins targeting mitochondrial complex I, such as 1-methyl-4-phenyl-1,2,3,6-tetrahydropyridine (MPTP), can result in mitochondrial damage and an imbalance in intracellular homeostasis leading to the death of nigrostriatal neurons [13]. Mutations in mitochondrial complex I components have also been reported to be related to neurodegenerative diseases, including PD and Leigh syndrome [14, 15]. Complex I dysfunction is critical in PD pathogenesis and is correlated with the degeneration of dopaminergic neurons in the substantia nigra pars compacta (SNpc). Complex I defects and increased oxidative damage are consistent features of both sporadic and familial PD forms [16]. NDUFS7 (homolog of NDUF-7 in *C. elegans*) is one of the important subunits of mitochondrial complex I, and we have

[1]Jiangsu Key Laboratory of Druggability of Biopharmaceuticals, State Key Laboratory of Natural Medicines, School of Life Science and Technology, China Pharmaceutical University, Nanjing 211198, China and [2]Department of Chemistry, China Pharmaceutical University, Nanjing 211198, China
Correspondence: Wen-bing Yao (wbyao@cpu.edu.cn) or Xiang-dong Gao (xdgao@cpu.edu.cn) or Song Chen (ChenS@cpu.edu.cn)
These authors contributed equally: Jie Shen, Qian Zha, Qian-hua Yang

Received: 26 June 2022 Accepted: 16 October 2022
Published online: 10 November 2022

previously reported that NDUF-7 dysfunction in nematodes can lead to dopaminergic neurodegeneration [17]. In recent years, hypoxic treatment has been reported to be able to reverse neurodegenerative disease in a mouse model of Leigh syndrome [18]. In our previous publication, we reported that inactivation of von Hippel–Lindau (VHL), one of the hypoxia pathway regulators, can effectively alleviate the abnormalities of dopaminergic neurons in *C. elegans* [17]. However, the specific effects of VHL loss and the underlying mechanism in mammalian PD models remain unexplored.

The aims of this study were to determine the protective effects of the loss of VHL against dopaminergic neurodegeneration in *C. elegans* and mammals mechanistically by regulating the Dishevelled-2 (DVL-2)/β-catenin axis, and to provide evidence that genetic and pharmacological targeting of VHL/DVL-2 can preserve dopaminergic neurons in experimental parkinsonism.

MATERIALS AND METHODS

Materials

MPTP, 1-methyl-4-phenylpyridinium (MPP^+), 3-(4,5-dimethylthiazol-2-yl)-2,5-diphenyltetrazolium bromide (MTT), and Compound 3289–8625 (DVL-2 inhibitor) were purchased from Sigma–Aldrich (St. Louis, USA). Dulbecco's modified Eagle's medium (DMEM) high glucose medium and fetal bovine serum (FBS) were purchased from Gibco Life Technologies (Grand Island, USA). hs-*VHL*-siRNA and mus-*Vhl*-siRNA were purchased from Biomics Biotechnologies (Nantong, China). KC7F2, XAV-939, VH298, and FG-4592 were purchased from MedChemExpress (Shanghai, China). Compound 15i was prepared as previously described [19]. The pcDNA3.1(+)-NDUFS7 Q208STOP recombination plasmid and pcDNA3.1(+)-DVL-2 recombination plasmid were constructed by GenScript Biotech Corporation (Nanjing, China). Entranster™-in vivo transfection reagent was purchased from Engreen Biosystem Co., Ltd. (Beijing, China). Biotin-labeled DDFs, Tat and Tat-DDF-2 were synthesized by GL Biochem Ltd. (Shanghai, China). Dynabeads™ MyOne™ Streptavidin C1 was purchased from Thermo Scientific (Waltham, USA). Human VHL recombinant protein was purchased from Abcam (Cambridge, UK).

Mice and treatments

All male mice (8 weeks old) were purchased from Vital River Laboratory Animal Technology Co., Ltd. (Beijing, China). The animal experiments were approved by the Institutional Animal Care and Use Committee of China Pharmaceutical University. All mice were housed in a light/dark cycle (12 h/12 h) with free access to water and food.

For the in vivo genetic inhibition of VHL, mice were randomly divided into the following groups: the Saline + Non, Saline + AAV-negative control (NC)-shRNA, Saline + AAV-*Vhl*-shRNA, MPTP + Non, MPTP + AAV-NC-shRNA, and MPTP + AAV-*Vhl*-shRNA groups. The "Saline + Non" group represented mice that were not treated with shRNA at the same time as saline treatment, and the "MPTP + Non" group represented mice that were not treated with shRNA at the same time as MPTP treatment. AAV (HanBio, Shanghai, China) was injected into each lateral ventricle (0.5 mm posterior to bregma and 1.0 mm lateral to the midline) of the mice using a stereotaxic apparatus (RWD Life Science Co., Ltd., Shenzhen, China). Thirty days later, MPTP (30 $mg{\cdot}kg^{-1}$ per day) was injected intraperitoneally once a day for five consecutive days. Behavioral experiments were conducted on the D1, D3, D7, D14, and D21 after the last injection. Then, the mice were sacrificed on the D22. siRNA sequences were as follows: mus-*Vhl*-siRNA: sense 5′-CAUUGCCAG UGUAUACCCUdTdT-3′, antisense 5′-AGGGUAUACACUGGCAAUG dTdT-3′.

For the in vivo overexpression of DVL-2, mice were randomly assigned to four groups: the Saline + pcDNA3.1(+), Saline + pcDNA3.1(+)-DVL-2, MPTP + pcDNA3.1(+), and MPTP + pcDNA3.1(+)-DVL-2 groups. Mice received intracerebroventricular (ICV) injection of pcDNA3.1(+)-DVL-2 plasmid or pcDNA3.1(+) empty vector using Entranster™-in vivo DNA transfection reagent according to the manufacturer's instructions. Briefly, 2.5 μL of plasmid or 2.5 μL of empty vector was added to 5 μL of Entranster™-in vivo DNA transfection reagent at room temperature. Then, the Entranster™-in vivo plasmid mixture was injected (ICV) before and after intraperitoneal injection of MPTP (20 $mg{\cdot}kg^{-1}$, 2-h intervals, 4 doses). The mice were sacrificed on the D10 for biochemical tests.

For the in vivo blockade experiments, mice were randomly allocated to four groups: the Saline + NC-siRNA + dimethyl sulfoxide (DMSO), MPTP + NC-siRNA + DMSO, MPTP + *Vhl*-siRNA + DMSO, and MPTP + *Vhl*-siRNA + XAV-939 groups. In vivo transfection experiments were executed by two ICV injections of *Vhl*-siRNA before and after intraperitoneal injection of MPTP (20 $mg{\cdot}kg^{-1}$, 2-h intervals, 4 doses) on the D3. Briefly, 2.5 μg of *Vhl*-siRNA was dissolved in 2.5 μL of endotoxin-free pure water and then mixed with 1.25 μL of Entranster™-in vivo RNA transfection reagent at a ratio of 2:1. For the small molecule inhibitor group, XAV-939 (30 $mg{\cdot}kg^{-1}$) was injected intraperitoneally on the D1, D2, D4, and D5. The mice were sacrificed on the D10 for biochemical tests.

For the in vivo activity evaluation of Tat-DDF-2, mice were randomly allocated to four groups: the Vehicle, MPTP, MPTP + Tat, and MPTP + Tat-DDF-2 groups. Mice were intraperitoneally injected with Tat or Tat-DDF-2 (1 $mg{\cdot}kg^{-1}{\cdot}d^{-1}$) from the D1 to the D6. MPTP (20 $mg{\cdot}kg^{-1}$, 2-h intervals, 4 doses) was injected intraperitoneally on the D2. Behavioral experiments were conducted on the D7. Then, the mice were sacrificed on the D9 for biochemical tests.

C. elegans strains and treatments

The genotypes of the *C. elegans* strains used in this study are as follows: *zcIs9 V; otIs181 III, nduf-7(et19) I; zcIs9 V; otIs181 III*, and *nduf-7(et19) I; zcIs9 V; otIs181 III; vhl-1(ok161) X* [17]. The genetic marker *zcIs9 [hsp-60p::GFP]* was used to monitor the mitochondrial unfolded protein response, and *otIs181 [dat-1p::mCherry+ttx-3p::mCherry]* was used to mark all 4 pairs of dopamine neurons (2 pairs of CEP neurons, one pair of ADE neurons and one pair of PDE neurons) and one pair of nondopaminergic AIY neurons. *nduf-7(et19)* is a nonsense mutation that removes the last 5 highly conserved amino acids of NDUF-7. *vhl-1(ok161)* is a genetic deletion that causes loss of function of VHL. *C. elegans* were cultured and maintained at 20 °C on standard Nematode Growth Medium agar plates seeded with *Escherichia coli* (*E. coli*) OP50. After incubation at 20 °C on standard Nematode Growth Medium agar plates seeded with *E. coli* OP50, synchronized worms at the L1 stage were washed twice in M9 buffer and then treated with VH298, FG-4592 or Compound 15i prior to exposure to 1 mM MPP^+ at 20 °C. ADE neurons were recorded at the L4 stage by a confocal laser scanning microscope (Zeiss, Jena, Germany).

Cell culture and treatments

SH-SY5Y cells were cultured in DMEM containing 10% FBS and penicillin/streptomycin at 37 °C under 5% CO_2 and differentiated in DMEM with 10 μM retinoic acid (MedChemExpress) for 3 d and 80 nM 12-O-tetradecanoylphorbol-13-acetate (MedChemExpress) for another 3 d. For genetic inhibition or plasmid transfection, the cells were transfected with *VHL*-siRNA or pcDNA3.1(+)-NDUFS7 Q208STOP recombination plasmid using Lipofectamine 3000 (Invitrogen, Carlsbad, USA) according to the manufacturer's instructions. For pharmacological inhibition experiments, cells were preincubated with VH298, FG-4592 or Compound 15i for 1 h and further treated with MPP^+ (150 μM) or rotenone (0.15 μM). For in vitro blockade experiments, KC7F2 (5 μM) and XAV-939 (5 nM) were used. For the in vitro activity evaluation of Tat-DDF-2, differentiated SH-SY5Y cells were incubated with Tat-DDF-2 (2.5, 5, 10, 20, and 40 μM) and treated with MPP^+ (150 μM). The *VHL*-

siRNA sequences were as follows: sense 5′-GGCUCAACUUCGAC GGCGAdTdT-3′, antisense 5′-UCGCCGUCGAAGUUGAGCCdTdT-3′.

Open field test
The test apparatus was composed of an open field box and a video tracking system. The inside of the open field box was painted with a light color and separated with partitions into four squares of congruence. The mice were placed in the center of the open field boxes and allowed to explore for 5 min under dim light. The apparatus was thoroughly cleaned with diluted 75% ethanol between each trial. The video tracking system (ANY-Maze software) was used to record and collect data.

Rotation test
For the rotation test, the mice were placed on the rotarod cylinder at 5 rpm, and the durations were recorded. The trial ended if the mice fell off the rungs, gripped the apparatus or rotated twice in a row without trying to walk on the rung. Motor test data are presented as the duration on the rotarod.

Pole test
The pole was made of a metal rod with a length of 600 mm and a diameter of 10 mm. The pole was wrapped with bandage gauze to prevent the mice from slipping, and a ball with a diameter of 20 mm was fixed on the top of the pole. Mice were placed near the top of the pole facing upward, and the time taken to climb from the top of pole to the bottom was recorded.

Beam walking test
A 1200-mm metal beam with a diameter of 10 mm was fixed at a position 200 mm above the ground. A light-tight carton was placed at one end of the beam as the end point, and mice were placed on the other end of the beam. The time taken to reach the light-tight carton was recorded.

Immunohistochemistry
Mouse brains were collected and fixed for 24 h in 4% paraformaldehyde. Then, the brains were embedded in paraffin, and 5-μm coronal sections were successively cut with a microtome in the SNpc and ST. After dewaxing and antigen repair, sections were blocked with 3% hydrogen peroxide to block endogenous catalase. The sections were incubated with an antibody against tyrosine hydroxylase (TH; Cell Signaling Technology, Beverly, USA) followed by incubation with secondary antibody (Cell Signaling Technology). After developing with 3,3′-diaminobenzidine peroxidase substrate (Dako, Copenhagen, Denmark), the nuclei were stained with hematoxylin and dehydrated to seal the sections. The number of TH neurons in the SNpc was quantified using unbiased stereological analysis. The TH fiber density in the ST was digitally scanned using Nanozoomer Digital Pathology (Hamamatsu Photonics Co., Ltd, Hamamatsu, Japan) and measured using ImageJ software.

Immunofluorescence
Paraffin sections of brain tissue were dewaxed in different concentrations of organic reagents, and antigen retrieval was performed with ethylenediaminetetraacetic acid in a microwave oven. Tissue slices were incubated with an autofluorescence quencher for 5 min to eliminate autofluorescence. The primary antibody (anti-α-synuclein, BD Biosciences, Franklin Lakes, USA; anti-β-catenin, Cell Signaling Technology) diluted in 5% bovine serum albumin was added to cover the tissue after the slices were dried. Then, the slices were placed in a wet box and incubated overnight at 4 °C, and the immunoreaction was detected using a fluorescence-conjugated secondary antibody. The nuclei were stained with 4′,6-diamidino-2-phenylindole (DAPI), and the tissue sections were sealed with an anti-fluorescence quencher. Images were captured using a confocal laser scanning microscope (Zeiss).

Hoechst/PI assay
Differentiated SH-SY5Y cells were seeded on 6-well plates and transfected with *VHL*-siRNA with or without MPP^+ interference for 48 h. Then, 7 mM Hoechst 33342 and 2 mM PI (Beyotime Institute of Biotechnology, Shanghai, China) were added. The images were taken using a confocal laser scanning microscope (Zeiss). Quantitative analysis was conducted using ImageJ software.

Cell viability assay
The cells were cultured on 96-well plates. After the treatments, cells were incubated with 0.5 mg·mL^{-1} MTT for 4 h at 37 °C. Subsequently, the supernatants were removed, 150 μL of DMSO was added to each well, and the absorbance was quantified at a test wavelength of 570 nm and a reference wavelength of 630 nm.

Annexin V-FITC/PI assay
An Annexin V-FITC/PI assay kit (Beyotime Institute of Biotechnology) was used to detect the cell apoptosis level. After intervention, the cells were digested and centrifuged at 1500 r·min^{-1} for 5 min. Then, the cells were incubated with 195 μL of binding buffer, stained with 5 μL of Annexin V-FITC and 10 μL of PI for 20 min, detected by flow cytometry (BD Biosciences) and analyzed with FlowJo software.

Proximity ligation assay (PLA)
PLA was performed according to the manufacturer's protocol (Sigma–Aldrich). The differentiated cells were washed with cold PBS and fixed in 4% paraformaldehyde for 20 min, followed by permeabilization with 0.1% Triton X-100 for 10 min. Then, the cells were blocked with Duolink Blocking Solution at 37 °C for 1 h. The primary antibodies to detect VHL and DVL-2 were added and incubated overnight at 4 °C, followed by incubation with the two PLA probes (Anti-Rabbit PLUS and Anti-Mouse MINUS). The ligation and polymerization steps were conducted at 37 °C, followed by incubation with Duolink In Situ Mounting Medium with DAPI. Fluorescence images were acquired using a confocal laser scanning microscope (Zeiss).

Analysis of mitochondrial morphology
Differentiated SH-SY5Y cells were incubated with a working solution of the MitoTracker Red probe (GenMed Scientifics Inc., Shanghai, China) for 20 min at 37 °C in the dark. The cells were washed, and images were acquired using a confocal laser scanning microscope (Zeiss). The parameter examined was the mitochondrial length.

Analysis of mitochondrial membrane potential
The mitochondrial membrane potential was detected using a JC-1 fluorescence probe (Beyotime Institute of Biotechnology). The cells were incubated with JC-1 solution for 20 min at 37 °C. Then, the cells were washed twice with JC-1 buffer. Images were taken using a fluorescence microscope (Olympus, Tokyo, Japan). The ratio of red to green fluorescence represents the mitochondrial membrane potential.

Western blotting
Tissue samples were isolated from the SNpc and ST of the mouse brain. Proteins from tissue samples or SH-SY5Y cells were extracted using RIPA buffer (Beyotime Institute of Biotechnology) containing protease and phosphatase inhibitor cocktail (Thermo Scientific). Then, the solution was centrifuged at 12000 rpm for 20 min, and the soluble supernatant was collected. Protein levels were analyzed using Western blotting as previously described [20] with primary antibodies against TH, HIF-1α, β-catenin, DVL-2, p-S129 α-syn (Cell Signaling Technology), ubiquitin (UB), VHL (Santa Cruz Biotechnology, Dallas, USA), and β-actin (Abclonal, Wuhan, China). The appropriate HRP-conjugated secondary antibody (Cell Signaling Technology) and enhanced

chemiluminescence reagents (Millipore, Billerica, USA) were used, and the band intensities were quantified by densitometry analysis using ImageJ software.

Immunoprecipitation
Differentiated SH-SY5Y cells were seeded on 6-well plates and transfected with *VHL*-siRNA with or without MPP^+ interference for 48 h. The cell lysates were incubated with anti-DVL-2 antibody (Cell Signaling Technology) at 4 °C overnight. Then, the solution was incubated with protein A/G agarose beads (Santa Cruz Biotechnology) for 4 h at 4 °C. The solution was centrifuged at 1000 r·min^{-1} for 3 min, and the supernatant was discarded. The precipitate was washed 3 times with RIPA buffer for 5 min each wash. A total of 30 μL solution was left and analyzed using Western blotting with a primary antibody against UB (Santa Cruz Biotechnology).

RNAi feeding
RNAi feeding was performed as previously described [21]. The following primers (GenScript Biotech Corporation) were used in the experiments:
dsh-2 Forward: 5′-CGAGCTCAATCGTCAATGGGTCTAGAAG-3′
dsh-2 Reverse: 5′-GGGGTACCCTTCAGATATACTTGGCATTG-3′
bar-1 Forward: 5′-CGAGCTCGACCTGGATCCGAACCTAG-3′
bar-1 Reverse: 5′-GGGGTACCAAATCGACTATTCCTAGAAGG-3′

DNA/RNA isolation and quantitative PCR analysis
Intracellular DNA was extracted with a cell genome DNA extraction kit (Tiangen Biotech (Beijing) Co., Ltd., Beijing, China) following the manufacturer's instructions. Total RNA was isolated using an *EasyPure*® RNA kit (TransGen Biotech Co., Ltd., Beijing, China). RNA was isolated according to the manufacturer's instructions, and DNA was removed using RNase-Free DNase I (TransGen Biotech Co., Ltd.). cDNA was synthesized using HiScript II Reverse Transcriptase (Vazyme Biotech Co., Ltd., Nanjing, China). Relative mitochondrial DNA (mtDNA) copy number or gene expression levels were determined by real-time PCR using 2×ChamQ Universal SYBR qPCR Master Mix (Vazyme Biotech Co., Ltd.) and the QuantStudio™3 Real-Time PCR system. The $2^{-\Delta\Delta Ct}$ method was used to analyze the level of gene expression. The following primers (GenScript Biotech Corporation) were used in the experiments:
Human-specific primers:
DVL-2 Forward: 5′-GCCTATCCAGGTTCCTCCTC-3′
DVL-2 Reverse: 5′-AGAGCCAGTCAACCACATCC-3′
GAPDH Forward: 5′-CCACTCCTCCACCTTTGACG-3′
GAPDH Reverse: 5′-CCACCACCCTGTTGCTGTAG-3′
mtDNA Forward: 5′-CAAACCTACGCCAAAATCCA-3′
mtDNA Reverse: 5′-GAAATGAATGAGCCTACAGA-3′
nDNA Forward: 5′-ACGGACCAGAGCGAAAGCA-3′
nDNA Reverse: 5′-GACATCTAAGGGCATCACAGAC-3′
Mouse-specific primers:
Dvl-2 Forward: 5′-TGACAATGACGGTTCCAGTG-3′
Dvl-2 Reverse: 5′-GCGCTGGATACTGGTAGGAG-3′
Actb Forward: 5′-AGCCATGTACCTAGCCATCC-3′
Actb Reverse: 5′-TTTGATGTCACGCACGATTT-3′
C. elegans-specific primers:
dsh-2 Forward: 5′-GCGCAGTGCATCATCGAAAT-3′
dsh-2 Reverse: 5′-GCTAAACCAGACCCACTGCT-3′
bar-1 Forward: 5′-GAAGCACTAAATAGTAGCGGTGAA-3′
bar-1 Reverse: 5′-TTCTGGATACATTGCTGGTGGG-3′
gpd-1 Forward: 5′-TAACTTCGGTATCATCGAAGGACTC-3′
gpd-1 Reverse: 5′-GACGGAAACATCTGGTGTAGGGA-3′

Pull-down assay
SH-SY5Y cell lysates were incubated with biotin-labeled DDFs overnight at 4 °C using gentle rotation. Dynabeads™ MyOne™ Streptavidin C1 was added the next day and incubated for 1 h at room temperature using gentle rotation. The magnetic bead-protein complex was adsorbed by a magnetic stand and washed with PBS three times. Then, Western blotting was performed to analyze the level of VHL. Cell lysates can be replaced by human VHL recombinant protein in the pull-down assay in this study.

Statistical analysis
All data were analyzed using GraphPad Prism 8 software. Data are presented as the mean ± standard error of the mean (SEM). Unpaired two-tailed Student's *t* tests and one-way or two-way analysis of variance (ANOVA) followed by Tukey's multiple comparisons test were used to assess the statistical significance. P values < 0.05 were considered significant.

RESULTS

Behavioral and pathological abnormalities in mice with PD can be rescued by genetic inhibition of VHL
In this study, first, the effective mus-*Vhl*-siRNA fragment was screened for follow-up experiments (Supplementary Fig. S1a, b) and AAV-*Vhl*-shRNA was constructed. AAV-*Vhl*-shRNA was injected into the lateral ventricle in the brains of mice. Then the mice were injected with MPTP (30 mg·kg^{-1}) intraperitoneally for 5 consecutive days to establish subacute PD model mice. After the last MPTP injection, we tested the mice with a battery of behavioral and biochemical assays to analyze the behavioral changes and PD-related pathological characteristics of the mice (Fig. 1a). In the open field test, we found significant declines in the total distance traveled, the distance traveled in the center zone and the time spent in the center zone (Fig. 1b and Supplementary Fig. S2a–c) in the MPTP-injected mice, which were relieved by interference with VHL expression in the brains of mice. The rotarod test (Fig. 1c) and pole test (Supplementary Fig. S2d) showed that interference with VHL expression in the brains of MPTP-injected mice alleviated the behavioral defects. The decreased ability of mice to balance induced by MPTP injection can also be remitted by RNA interference-mediated inhibition of VHL expression (Supplementary Fig. S2e). MPTP-induced reductions in TH immunoreactivity in the SNpc (Fig. 1d, e) and ST (Fig. 1f, g) were rescued by interference with VHL expression in the brains of mice. Western blotting analysis confirmed that injecting AAV-*Vhl*-shRNA in the lateral ventricle can interfere with the expression of VHL in the SNpc and ST (Supplementary Fig. S3a–c), and interference with VHL expression in the brains of mice increased TH expression in the SNpc and ST (Fig. 1h–j). MPTP-induced α-syn pathology was ameliorated by interference with VHL (Supplementary Fig. S4a–f).

HIF is not essential for the reversal of experimental parkinsonism by VHL inactivation
To study the effects of the inhibition of the *VHL* gene on the apoptosis and degeneration of dopaminergic nerve cells caused by mitochondrial dysfunction, a dopaminergic nerve injury model was induced by MPP^+. MPP^+ can induce mitochondrial dysfunction by disturbing mitochondrial complex I in cells, subsequently resulting in the degeneration and apoptosis of dopaminergic nerve cells [22]. First, the effective hs-*VHL*-siRNA fragment was screened for follow-up experiments (Supplementary Fig. S5a, b). The results of Hoechst/PI staining showed that transfection of *VHL*-siRNA into differentiated SH-SY5Y cells alleviated the death of dopamine neurons induced by MPP^+ (Fig. 2a, b). The decreased TH expression in dopaminergic nerve cells induced by MPP^+ can be relieved by interfering with the expression of VHL in the cells (Fig. 2c, d). Inhibition of VHL in differentiated SH-SY5Y cells ameliorated MPP^+-induced mitochondrial damage (Supplementary Fig. S6a–d). In addition, we used the VHL inhibitor VH298 [23], the HIF hydroxylase PHD inhibitor FG-4592 [24] and Compound 15i [19] to further explore the mechanisms. Interestingly, we found

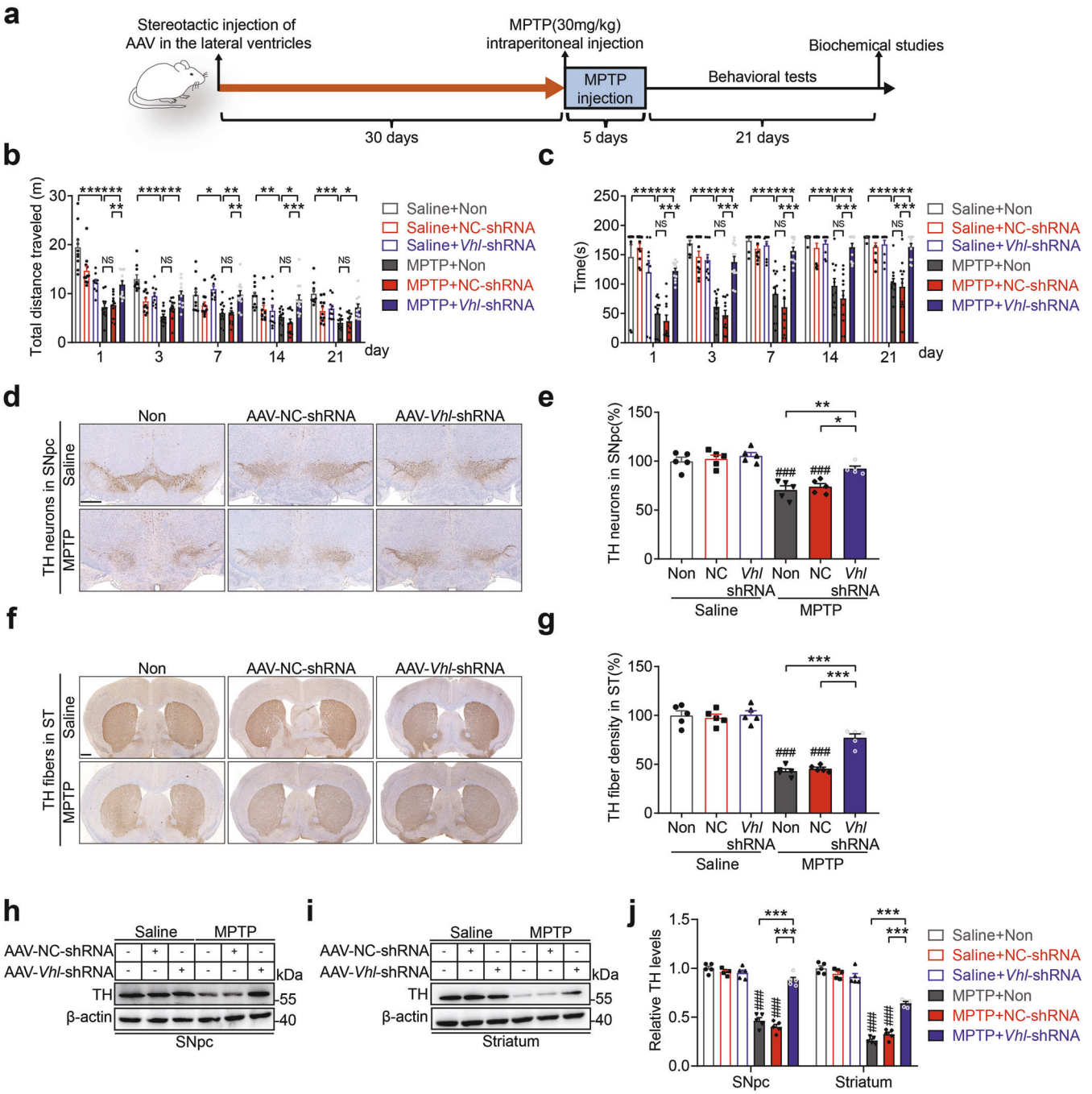

Fig. 1 VHL knockdown prevents behavioral and pathological abnormalities in PD model mice. a Procedure diagram of the animal experimental design. **b**, **c** Behavioral experiments after the last saline or MPTP intraperitoneal injection. Data are the mean ±SEM; Saline + Non group: $n = 10$ mice; Saline + AAV-NC-shRNA group: $n = 11$ mice; Saline + AAV-*Vhl*-shRNA group: $n = 10$ mice; MPTP + Non group: $n = 11$ mice; MPTP + AAV-NC-shRNA group: $n = 11$ mice; MPTP + AAV-*Vhl*-shRNA group: $n = 12$ mice; statistical significance was determined using two-way ANOVA followed by Tukey's correction. **b** The total distance traveled in the open field test. **c** Time spent on the rotarod. **d** Representative images from coronal sections containing TH-positive neurons in the SNpc. Scale bar, 500 μm. **e** Unbiased stereology counts of TH-positive neurons in the SNpc. Data are the mean ± SEM; $n = 5$; statistical significance was determined by using one-way ANOVA followed by Tukey's correction. **f** Representative images of TH fibers in the ST region. Scale bar, 500 μm. **g** Quantification of the TH fiber density in the ST region using ImageJ software. Data are the mean ± SEM; $n = 5$; statistical significance was determined by using one-way ANOVA followed by Tukey's correction. Representative immunoblots of TH and β-actin in the SNpc (**h**) and ST (**i**). **j** Quantification of TH levels in the SNpc and ST normalized to β-actin. Data are the mean ± SEM; $n = 5$; statistical significance was determined by using one-way ANOVA followed by Tukey's correction. $^{###}P < 0.001$ vs Saline + Non group. $^{*}P < 0.05$, $^{**}P < 0.01$, $^{***}P < 0.001$. NS not significant.

that VH298 alleviated the decrease in dopaminergic neuron viability induced by MPP^+, while FG-4592 and Compound 15i had no significant alleviating effect on the decrease in cell viability (Fig. 2e–g). We obtained similar results in the dopaminergic neuron injury model induced by rotenone (Supplementary Fig. S7a, b). We also used these three inhibitors in an MPP^+-induced *C. elegans* PD model. VH298-treated *C. elegans* showed significant alleviation of ADE neurodegeneration, while the

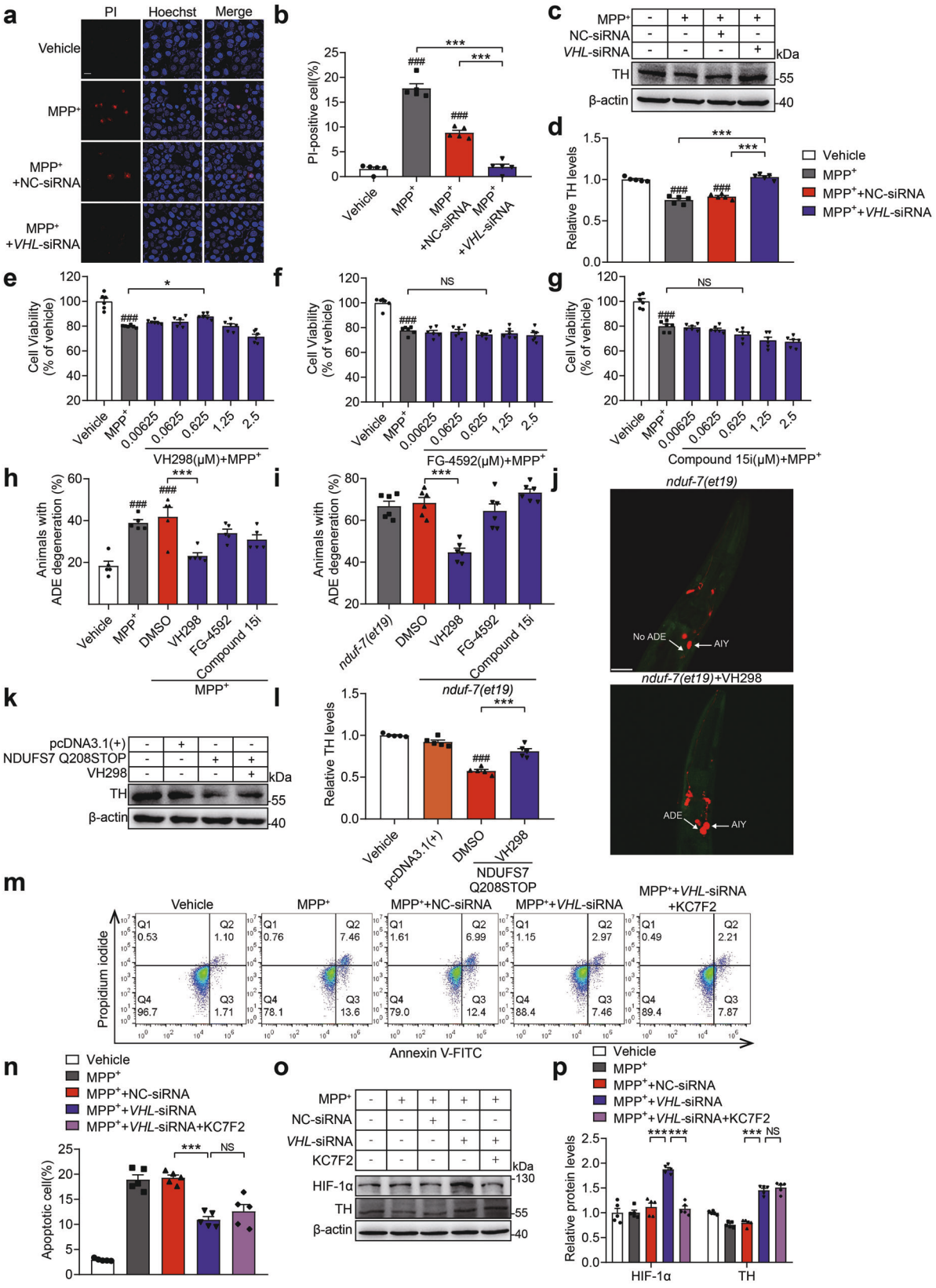

inhibitor FG-4592 and Compound 15i had no significant alleviating effect (Fig. 2h). *NDUFS7* is a gene in the nucleus, and its encoded protein participates in the formation of mitochondrial respiratory chain complex I. Previously, we found that *nduf-7* mutants can cause the degeneration of dopaminergic neurons in *C. elegans* [17]. Thus, we tested whether three inhibitors, VH298, FG-4592, and Compound 15i, can rescue dopamine neurodegeneration phenotypes in *C. elegans nduf-7(et19)* mutants.

Fig. 2 Genetic and pharmacological inhibition of VHL alleviates parkinsonian toxicant-induced neurodegeneration in cell and nematode models. a Representative images of Hoechst/PI staining from differentiated SH-SY5Y cells transfected with NC-siRNA or *VHL*-siRNA and further incubated with MPP^+ (150 μM) for 48 h. Scale bar, 20 μm. **b** Quantification of cell death. Data are the mean ± SEM; $n = 5$; statistical significance was determined by using one-way ANOVA followed by Tukey's correction. **c** Representative immunoblots of TH and β-actin. **d** Quantification of TH levels normalized to β-actin. Data are the mean ± SEM; $n = 5$; statistical significance was determined by using one-way ANOVA followed by Tukey's correction. **e**–**g** Quantification of cell viability in the MPP^+-induced injury model preincubated with VH298 (VHL inhibitor; **e**), FG-4592 (PHD inhibitor; **f**) or Compound 15i (PHD inhibitor; **g**) for 1 h and further treated with MPP^+ (150 μM). Data are the mean ± SEM; $n = 6$; statistical significance was determined by using one-way ANOVA followed by Tukey's correction. **h** Quantification of ADE neurodegeneration in L4-stage wild-type *C. elegans* treated with VH298, FG-4592 and Compound 15i prior to exposure to MPP^+ (1 mM). Data are the mean ± SEM; $n = 5$ plates (20–35 worms per plate); statistical significance was determined by using one-way ANOVA followed by Tukey's correction. **i** Quantification of ADE neurodegeneration in L4-stage *nduf-7(et19)* mutants of *C. elegans* treated with VH298, FG-4592 and Compound 15i. Data are the mean ± SEM; $n = 6$ plates (20–35 worms per plate); statistical significance was determined by using one-way ANOVA followed by Tukey's correction. **j** Representative images of L4-stage *nduf-7(et19)* incubated with DMSO or VH298. Scale bar, 20 μm. **k** Representative immunoblots of TH and β-actin from differentiated SH-SY5Y cells transfected with mutant plasmid pcDNA3.1(+)-NDUFS7 Q208STOP and further incubated with VH298 (0.625 μM) for 48 h. **l** Quantification of TH levels normalized to β-actin. Data are the mean ± SEM; $n = 5$; statistical significance was determined by using one-way ANOVA followed by Tukey's correction. **m** Representative flow cytometry pseudocolor plot of different groups of cells preincubated with/without KC7F2 (HIF-1α inhibitor) for 1 h. **n** Quantification of apoptotic cells. Data are the mean ± SEM; $n = 5$; statistical significance was determined by using one-way ANOVA followed by Tukey's correction. **o** Representative immunoblots of HIF-1α, TH and β-actin in different groups of cells preincubated with/without KC7F2 for 1 h. **p** Quantification of HIF-1α and TH levels normalized to β-actin. Data are the mean ± SEM; $n = 5$; statistical significance was determined by using one-way ANOVA followed by Tukey's correction. $^{###}P < 0.001$ vs vehicle group. $^*P < 0.05$, $^{***}P < 0.001$. NS not significant.

Consistent with the results of the MPP^+-induced worm model, ADE neurodegeneration caused by *nduf-7(et19)* mutants was relieved by treatment with VH298, while FG-4592 and Compound 15i had no significant protective effects against ADE neurodegeneration (Fig. 2i, j). Furthermore, we transfected differentiated SH-SY5Y cells with the mutant plasmid pcDNA3.1(+)-NDUFS7 Q208STOP, resulting in decreased expression levels of TH, and found that the expression levels of TH could also be normalized by VH298 treatment (Fig. 2k, l). These data showed that pharmacological inhibition of VHL but not HIF hydroxylases conferred protection against dopaminergic neurodegeneration, suggesting that a HIF-independent pathway mediates the downstream effects of VHL inhibition. To further confirm the results, we used the inhibitor KC7F2 [25], which can inhibit the protein synthesis of HIF-1α, thereby reducing the abundance of HIF-1α in the cell. Annexin V-FITC/PI staining followed by flow cytometry analysis showed that HIF-1α does not play a key VHL loss-dependent protective role in dopaminergic neuronal apoptosis caused by mitochondrial dysfunction (Fig. 2m, n). *VHL*-siRNA significantly increased the abundance of HIF-1α in differentiated SH-SY5Y cells and relieved the decreased TH expression in cells, while KC7F2 did not abolish the intervention effects of *VHL*-siRNA (Fig. 2o, p).

DVL-2 plays a crucial role in the neuroprotective effects conferred by VHL inactivation

In addition to HIF-1α, some other factors have been identified as VHL substrates [26–28]. To further analyze the interaction of endogenous VHL and substrate in the experimental model of PD, we used an in situ PLA. The enhancement of the interaction between VHL and DVL-2 was observed in situ following MPP^+ treatment compared with the basal levels (Fig. 3a, b), and thus, we speculated that DVL-2, as a HIF-independent target of VHL, may play a key role in experimental parkinsonism. We then verified that VHL inactivation can reduce the ubiquitination level of DVL-2 and inhibit the degradation of DVL-2 in cellular and mouse models of PD (Fig. 3c–j). Inhibition of VHL did not significantly influence mRNA levels of DVL-2 (Supplementary Fig. S8a, b). Furthermore, we found that the DVL-2 inhibitor Compound 3289–8625 eliminated the protective effect of *VHL*-siRNA on dopaminergic neuron degeneration (Fig. 3k, l). We also used RNAi to reduce the expression of the DVL-2 homolog DSH-2 in the *nduf-7(et19); vhl-1(ok161)* double-mutant *C. elegans* (Supplementary Fig. S9a) and found that the decrease in DSH-2 expression reduced the effect of VHL inhibition on the degeneration of dopaminergic neurons in L4-stage *C. elegans* (Fig. 3m).

In vivo overexpression of DVL-2 mimicking VHL inactivation protects against PD

We then overexpressed DVL-2 in vivo, mimicking VHL inactivation, and analyzed its effects on MPTP-induced PD-related pathological symptoms (Fig. 4a). Compared with the model group, the overexpression of DVL-2 significantly alleviated the MPTP-induced decrease in TH levels (Fig. 4b–d). VHL can mediate the ubiquitination and degeneration of DVL-2 [28], thereby destroying the stability of β-catenin [29]. After overexpression of DVL-2, the expression of β-catenin also increased significantly in the SNpc and ST in PD mice (Fig. 4e–h; Supplementary Fig. S10a).

Genetic targeting of VHL/DVL-2 protects against PD mechanistically by regulating the β-catenin axis

The data suggested that DVL-2 can alleviate the neurodegeneration of dopaminergic neurons via β-catenin. To confirm the contribution of β-catenin to the beneficial effects conferred by targeting VHL/DVL-2, we used the inhibitor XAV-939 [30], which can reduce the abundance of β-catenin by promoting its degradation. siRNA was used to induce VHL inactivation, thereby releasing DVL-2 in vitro and in vivo. In the MPP^+-induced PD cell models, XAV-939 attenuated the reduction in the apoptosis of model cells caused by VHL inactivation (Fig. 5a, b). We used XAV-939 to inhibit the levels of β-catenin in vivo and injected it intraperitoneally to analyze its effect on the VHL inactivation-induced alleviation of dopaminergic neuron degeneration (Fig. 5c). Compared with the *Vhl*-siRNA-treated group, the expression levels of TH in the SNpc and ST were significantly reduced in the mice cotreated with the inhibitor and *Vhl*-siRNA (Fig. 5d–j). XAV-939 partly abolished the protective effect conferred by VHL inactivation on the degeneration of dopaminergic neurons. Furthermore, we used RNAi to reduce the expression level of the *C. elegans* β-catenin homolog BAR-1 (Supplementary Fig. S9b) and found that knockdown of *bar-1* attenuated the neuroprotection of VHL inhibition in the L4-stage *nduf-7(et19); vhl-1(ok161)* double-mutant *C. elegans* (Fig. 5k). In the present study, regarding the mechanisms underlying the effects of targeting VHL/DVL-2 in the experimental model of PD, we confirmed that β-catenin played a key role in alleviating the degeneration of dopaminergic neurons caused by mitochondrial dysfunction. The data indicate that DVL-2/β-catenin is crucial for VHL inhibition to alleviate the neurodegeneration of dopaminergic neurons caused by mitochondrial dysfunction. Inhibiting the function of VHL may promote the stability of β-catenin by reducing the ubiquitination and degradation of DVL-2, thereby exerting a protective effect against the degeneration of dopaminergic neurons.

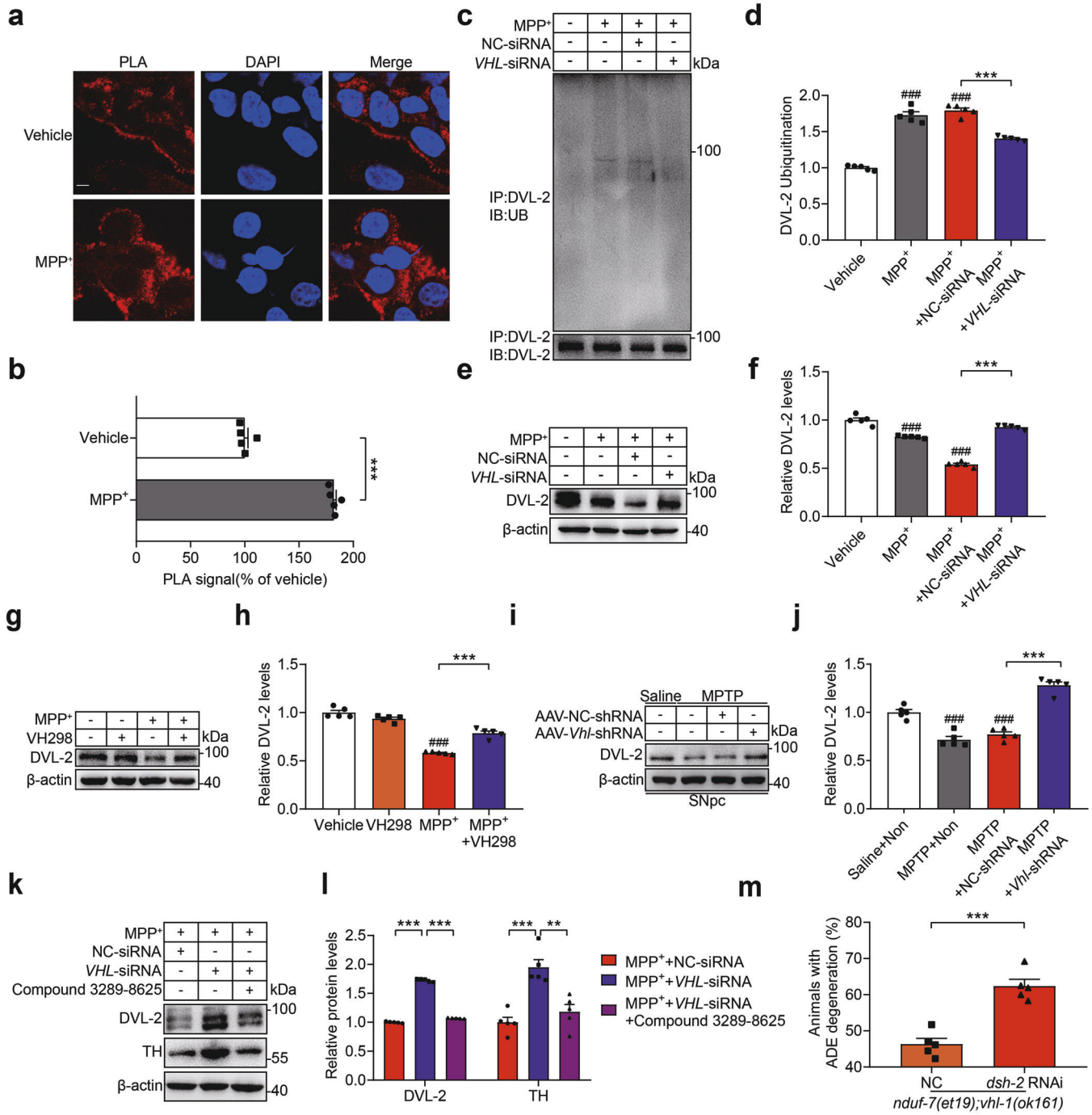

Fig. 3 Evidence for the role of DVL-2 in VHL inactivation conferring protection against PD. a Representative images of the PLA for VHL and DVL-2 in differentiated SH-SY5Y cells incubated with MPP^+ (150 μM) for 48 h. Scale bar, 5 μm. **b** Quantification of the PLA signal. Data are the mean ± SEM; $n = 5$; statistical significance was determined by using one-way ANOVA followed by Tukey's correction. **c** Representative immunoprecipitation of DVL-2 ubiquitination from differentiated SH-SY5Y cells transfected with NC-siRNA or *VHL*-siRNA and further incubated with MPP^+ (150 μM) for 48 h. **d** Quantification of DVL-2 ubiquitination. Data are the mean ± SEM; $n = 5$; statistical significance was determined by using one-way ANOVA followed by Tukey's correction. **e** Representative immunoblots of DVL-2 of genetic inhibition experiments in vitro. **f** Quantification of DVL-2 levels normalized to β-actin. Data are the mean ± SEM; $n = 5$; statistical significance was determined by using one-way ANOVA followed by Tukey's correction. **g** Representative immunoblots of DVL-2 and β-actin from pharmacological inhibition experiments in vitro. **h** Quantification of DVL-2 levels normalized to β-actin. Data are the mean ± SEM; $n = 5$; statistical significance was determined by using one-way ANOVA followed by Tukey's correction. **i** Representative immunoblots of DVL-2 and β-actin after genetic inhibition of VHL in vivo. **j** Quantification of DVL-2 levels normalized to β-actin. Data are the mean ± SEM; $n = 5$; statistical significance was determined by using one-way ANOVA followed by Tukey's correction. **k** Representative immunoblots of DVL-2, TH and β-actin. Compound 3289–8625 is the DVL-2 inhibitor. **l** Quantification of DVL-2 and TH levels normalized to β-actin. Data are the mean ± SEM; $n = 5$; statistical significance was determined by using one-way ANOVA followed by Tukey's correction. **m** Quantification of ADE neurodegeneration in L4-stage *nduf-7(et19); vhl-1(ok161)* double-mutant *C. elegans* after knocking down *dsh-2*. Data are the mean ± SEM; $n = 5$ plates (20–35 worms per plate); statistical significance was determined by using unpaired two-tailed Student's *t* test. $^{###}P < 0.001$ vs vehicle (or Saline + Non) group. $^{**}P < 0.01$, $^{***}P < 0.001$.

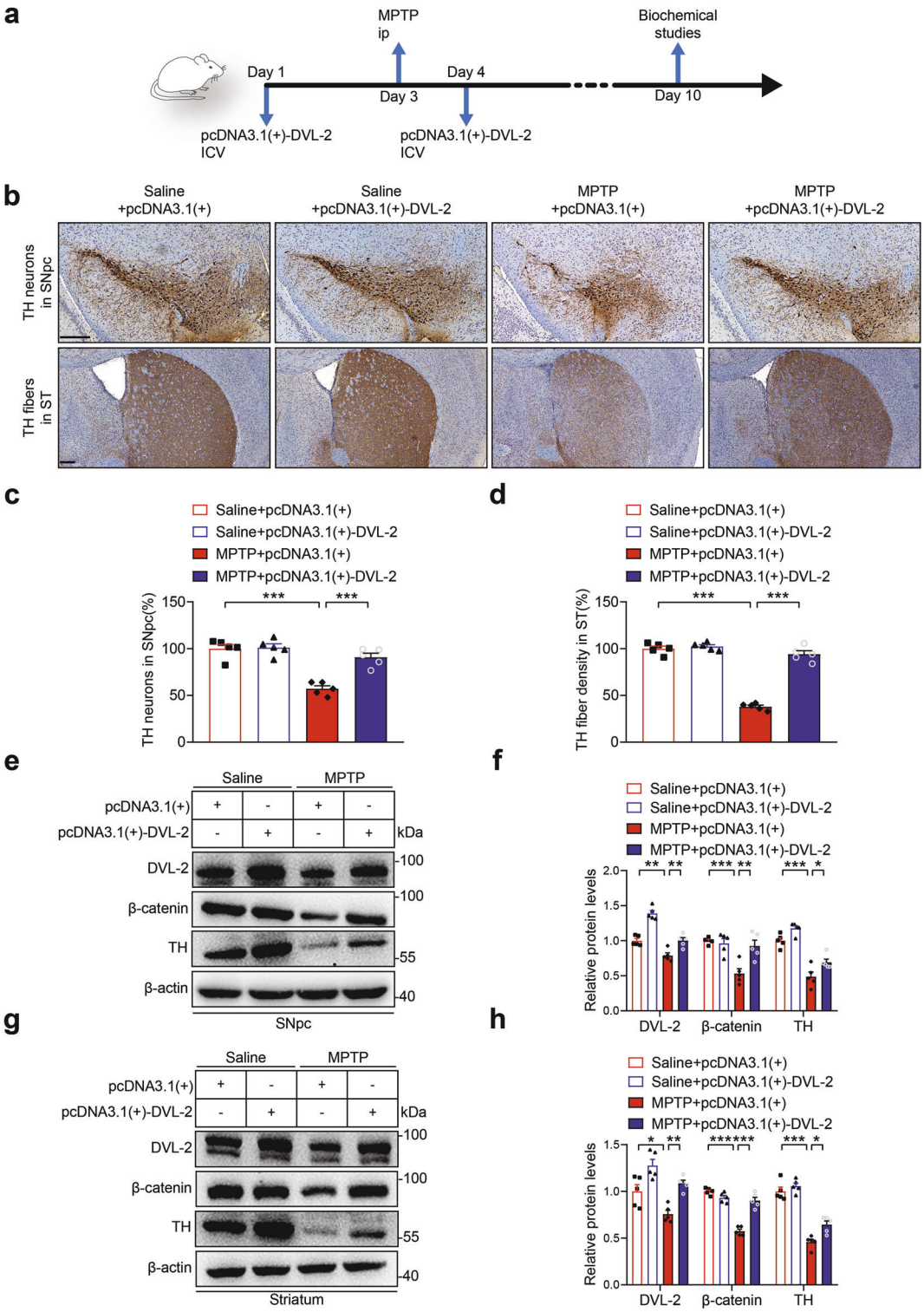

Fig. 4 DVL-2 overexpression mimics VHL inactivation followed by β-catenin axis enhancement and confers protection against PD. **a** Procedure diagram of the animal experimental design. **b** Representative images from coronal sections. Scale bar, 250 μm. **c**, **d** Unbiased stereology counts of TH-positive neurons in the SNpc and quantification of TH fiber in the ST. Data are the mean ± SEM; $n = 5$; statistical significance was determined by using one-way ANOVA followed by Tukey's correction. **e** Representative immunoblots of DVL-2, β-catenin, TH and β-actin in the SNpc. **f** Quantification of DVL-2, β-catenin and TH levels in the SNpc normalized to β-actin. Data are the mean ± SEM; $n = 5$; statistical significance was determined by using one-way ANOVA followed by Tukey's correction. **g** Representative immunoblots of DVL-2, β-catenin, TH and β-actin in the ST. **h** Quantification of DVL-2, β-catenin and TH levels in the ST normalized to β-actin. Data are the mean ± SEM; $n = 5$; statistical significance was determined by using one-way ANOVA followed by Tukey's correction. $^{*}P < 0.05$, $^{**}P < 0.01$, $^{***}P < 0.001$.

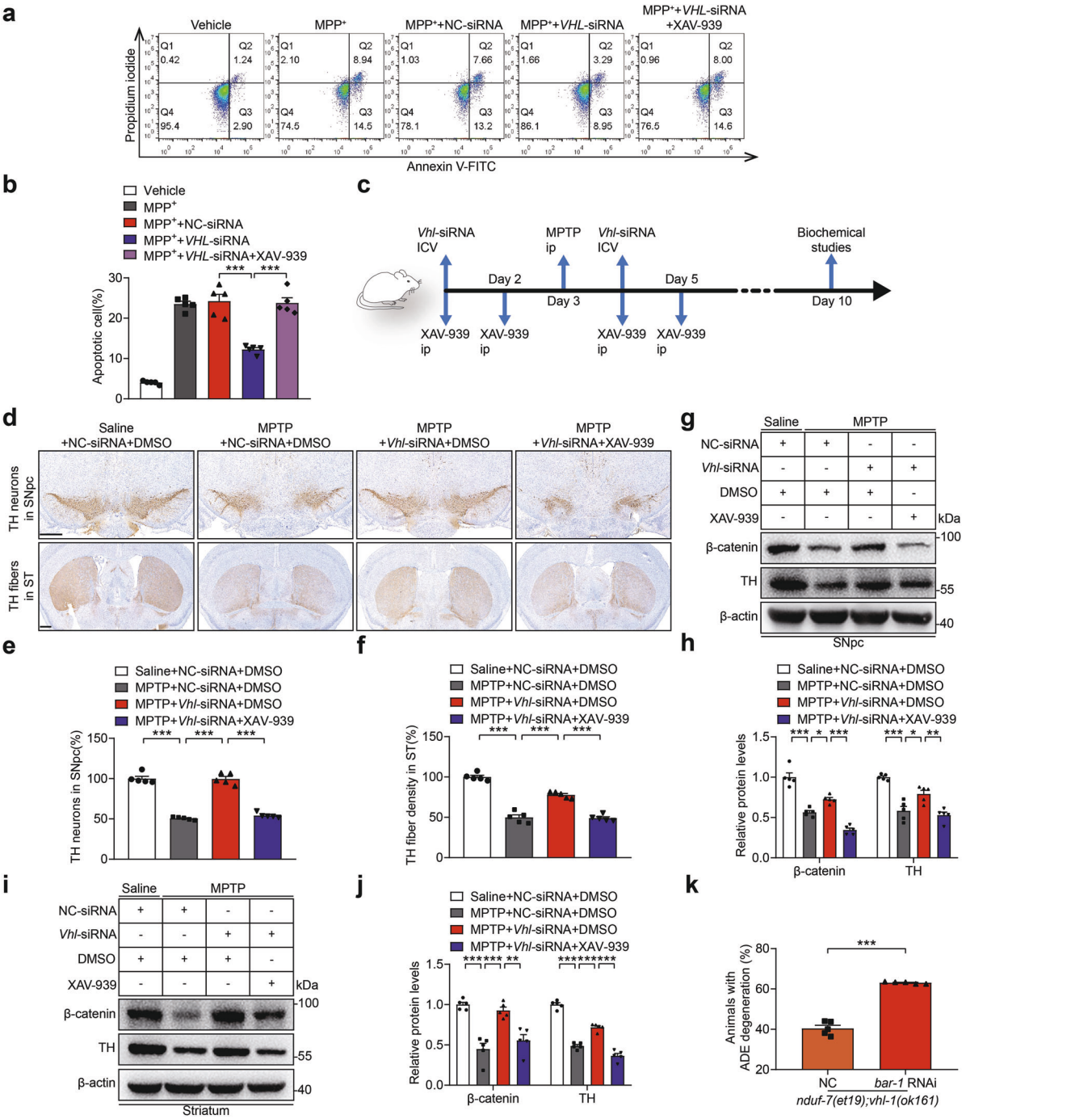

Fig. 5 β-catenin plays a key role in mediating the alleviation effects of VHL inhibition on the degeneration of dopaminergic neurons caused by mitochondrial dysfunction. a Representative flow cytometry pseudocolor plot of cells treated with/without NC-siRNA, *Vhl*-siRNA, XAV-939 (5 nM, β-catenin inhibitor) and MPP^+ (150 μM). **b** Quantification of apoptotic cells. Data are the mean ± SEM; $n = 5$; statistical significance was determined by using one-way ANOVA followed by Tukey's correction. **c** Procedure diagram of the animal experimental design. **d** Representative photos from coronal mesencephalon sections containing TH-positive neurons in the SNpc region and TH fiber in the ST region. Scale bar, 500 μm. Unbiased stereology counts of TH-positive neurons in the SNpc region (**e**) and quantification of TH fiber densities in the ST region (**f**) using ImageJ software. Data are the mean ± SEM; $n = 5$; statistical significance was determined by using one-way ANOVA followed by Tukey's correction. **g** Representative immunoblots of β-catenin, TH and β-actin in the SNpc region. **h** Quantification of β-catenin and TH levels in the SNpc region normalized to β-actin. Data are the mean ± SEM; $n = 5$; statistical significance was determined by using one-way ANOVA followed by Tukey's correction. **i** Representative immunoblots of β-catenin, TH and β-actin in the ST region. **j** Quantification of β-catenin and TH levels in the ST region normalized to β-actin. Data are the mean ± SEM; $n = 5$; statistical significance was determined by using one-way ANOVA followed by Tukey's correction. **k** Quantification of ADE neurodegeneration in L4-stage *nduf-7(et19); vhl-1(ok161)* double-mutant *C. elegans* after knocking down *bar-1*. Data are the mean ± SEM; $n = 5$ plates (20–35 worms per plate); statistical significance was determined by using unpaired two-tailed Student's *t* test. $^*P < 0.05$, $^{**}P < 0.01$, $^{***}P < 0.001$.

Pharmacological targeting of VHL/DVL-2 by a competing peptide preserves dopaminergic neurons in PD

A series of peptide DDFs, DVL-2-DEP-C fragments, based on the DEP-C region of DVL-2 were designed (Fig. 6a). The pull-down method was used to analyze the direct interaction between DDFs and VHL. First, the differentiated SH-SY5Y cell lysate was incubated with biotin-labeled DDFs. After the protein complex was pulled down by avidin magnetic beads, the VHL protein level was analyzed by Western blotting. The results showed that DDF-2, DDF-5, DDF-6 and DDF-8 had strong interactions with VHL (Fig. 6b, c). The pull-down verification of human VHL recombinant protein and biotin-labeled DDFs was consistent with the above results (Fig. 6d). To improve the efficiency of the peptide penetrating the blood–brain barrier and entering cells, DDF-2 linked to the cell-penetrating peptide Tat, named Tat-DDF-2, was designed and synthesized. The pharmacological potential of Tat-DDF-2 to protect against PD was evaluated in vitro and in vivo. The results showed that Tat-DDF-2 had a significant protective effect on the MPP^+-induced PD cell model (Fig. 6e). In addition, Tat-DDF-2 improved the expression level of TH in PD model cells. Compared with the model group, the levels of DVL-2 and β-catenin in the treated group were both increased (Fig. 6f, g). Tat-DDF-2 has also been shown to improve the pathological conditions and behavioral defects of the MPTP-induced PD mouse model. The experimental process is shown in Fig. 6h. The results of behavioral experiments, including the rotation test (Fig. 6i), pole test (Fig. 6j), and beam walking test (Fig. 6k), showed that Tat-DDF-2 alleviated the behavioral defects of MPTP-induced PD model mice. The immunohistochemistry results showed that Tat-DDF-2 can rescue the MPTP-induced reduction in TH immunoreactivity in the SNpc and ST (Fig. 6l–n) of the mouse brain. These data suggested that antagonizing the interaction of VHL/DVL-2 with a competing peptide may exert a protective effect similar to the protective effect of VHL inactivation against experimental parkinsonism.

DISCUSSION

PD is the second most common neurodegenerative disease after Alzheimer's disease, and in recent years, PD has become the fastest growing neurological disorder globally [31]. Unfortunately, effective treatments are still lacking, and new therapeutic targets and treatment strategies are urgently needed. We previously identified VHL, a key regulator in the hypoxia-related pathway, as a potential therapeutic target in dopaminergic neurodegeneration using *C. elegans* models. Based on our results, we propose that the evolutionarily conserved VHL/DVL-2 pathway might be a potential target for treating PD in both *C. elegans* and mammals and report that genetic and pharmacological targeting of VHL/DVL-2 can preserve dopaminergic neurons in experimental parkinsonism mechanistically by regulating the β-catenin axis.

Mitochondrial dysfunction in nerve cells has been widely studied as a key factor leading to PD [32, 33]. The impairment of mitochondrial complex I and changes in mitochondrial morphology were observed in substantia nigra dopaminergic neurons from PD patients, suggesting that the mitochondrial quality control system is defective in PD patient brains [34, 35]. MPTP, a byproduct of the synthesis of a meperidine analog with a potent heroin-like effect, can penetrate the blood–brain barrier and can be converted into MPP^+ in the brain by monoamine oxidase, which can specifically inhibit the activity of mitochondrial complex I, causing mitochondrial dysfunction that leads to the death of neurons [36]. In this study, we first validated the interventional effect of the inhibition of VHL function in a subacute PD mouse model induced by MPTP. The inhibition of VHL function can improve the autonomic activity of subacute PD model mice and can relieve the reduction in TH content in the SNpc and ST of mice. Thus, inhibition of VHL function can improve PD-like lesions in mice with subacute PD. Based on the MPP^+-induced cell models, siRNA targeting *VHL* can reduce the apoptosis levels of cell models and alleviate the abnormalities of TH levels. NDUFS7 is encoded by genes in the nucleus and participates in the formation of mitochondrial respiratory chain complex I, which is an important part of the hydrophobic subunit of complex I [37, 38]. Based on the *C. elegans* model, we found that mutation of *nduf-7* caused dopaminergic neurons to degenerate [17]. In this study, we also verified this phenomenon in mammalian cell models. Moreover, to some extent, an inhibitor of VHL can relieve dopaminergic neuron degeneration caused by NDUFS7 mutation. In addition, the nondopaminergic neurons were analyzed in our previous study, and we found that genetic deletion of the *C. elegans* ortholog of VHL markedly suppressed the effects of *nduf-7(et19)* in causing the loss of dopaminergic neurons, and the nondopaminergic neurons in the animals did not show significant impairment in all groups [17]. To further investigate the effects and mechanisms of VHL inactivation, conditional knockout of the *Vhl* gene in mice by technologies such as the Cre-loxP system may provide a more precise regulation and enable a more in-depth understanding of the effects of VHL inhibition on different types of neurons. Zhu et al. demonstrated that VHL promotes follicular helper T-cell differentiation via glycolytic-epigenetic control by using VHL conditional knockout mice [39]. Cargill et al. identified a novel role for VHL in mediating nephron progenitor differentiation through metabolic regulation in VHL conditional knockout mice [40]. VHL conditional knockout mice were used to study the effect of VHL deletion in renal epithelial cells on the development of clear-cell renal cell carcinoma by Nguyen-Tran et al. [41].

Under normal oxygen conditions, after HIF-1α is hydroxylated under the action of proline hydroxylase, VHL, as an E3 ubiquitin ligase, can target HIF-1α for ubiquitination and proteasome degradation, while the inhibition of VHL function can lead to the stabilization of HIF-1α and the activation of HIF-mediated genes, thereby activating related signaling pathways [42]. Interestingly, we have found a more important factor than HIF-1α for the neuronal protection mediated by VHL inhibition. In addition to HIF-1α, VHL can also promote the ubiquitination and degradation of DVL-2, thereby decreasing the level of β-catenin [28, 29]. Using a PLA assay, abnormal enhancement of the interaction between VHL and DVL-2 was observed in the PD model. Thus, we speculated that the DVL-2/β-catenin axis contributed to the beneficial effects of VHL inhibition against PD. KC7F2 is a small molecule inhibitor of HIF-1α, and XAV-939 is a small molecule inhibitor of β-catenin. We used these two inhibitors to study the roles of HIF-1α and β-catenin in the neuroprotection mediated by VHL inhibition. In the in vitro experiments, the results showed that the neuroprotective role of targeting VHL may be more closely tied to the β-catenin-related pathway. The in vivo data confirmed that β-catenin played a crucial role in the protective action of VHL inactivation. Similar to the β-catenin inhibitor, the DVL-2 inhibitor also attenuated the protective effect of *VHL*-siRNA. Consistent with the results of the mammalian system, in *C. elegans*, our results showed that both a reduction in the expression of DSH-2 or the expression of BAR-1 in *nduf-7(et19); vhl-1(ok161)* mutant *C. elegans* can significantly reduce the effect of VHL inhibition on dopaminergic neurons. Among HIF-independent pathways downstream of VHL, the DVL-2/β-catenin axis plays an evolutionarily conserved role in protection against PD-like neurodegeneration. Furthermore, we showed that overexpression of DVL-2 in the mouse brain can exert a similar anti-PD action to VHL inactivation. In DVL, there are three essential domains, namely, DIX, PDZ, and DEP, and the DEP domain of DVL-2 plays a crucial role in its binding with VHL [43]. Based on these findings, a competing peptide designed for targeting VHL/DVL-2 also showed pharmacological potential for protection against PD-like syndrome.

In summary, in this paper, we demonstrate that inactivation of VHL protein protects against experimental parkinsonism in both *C.*

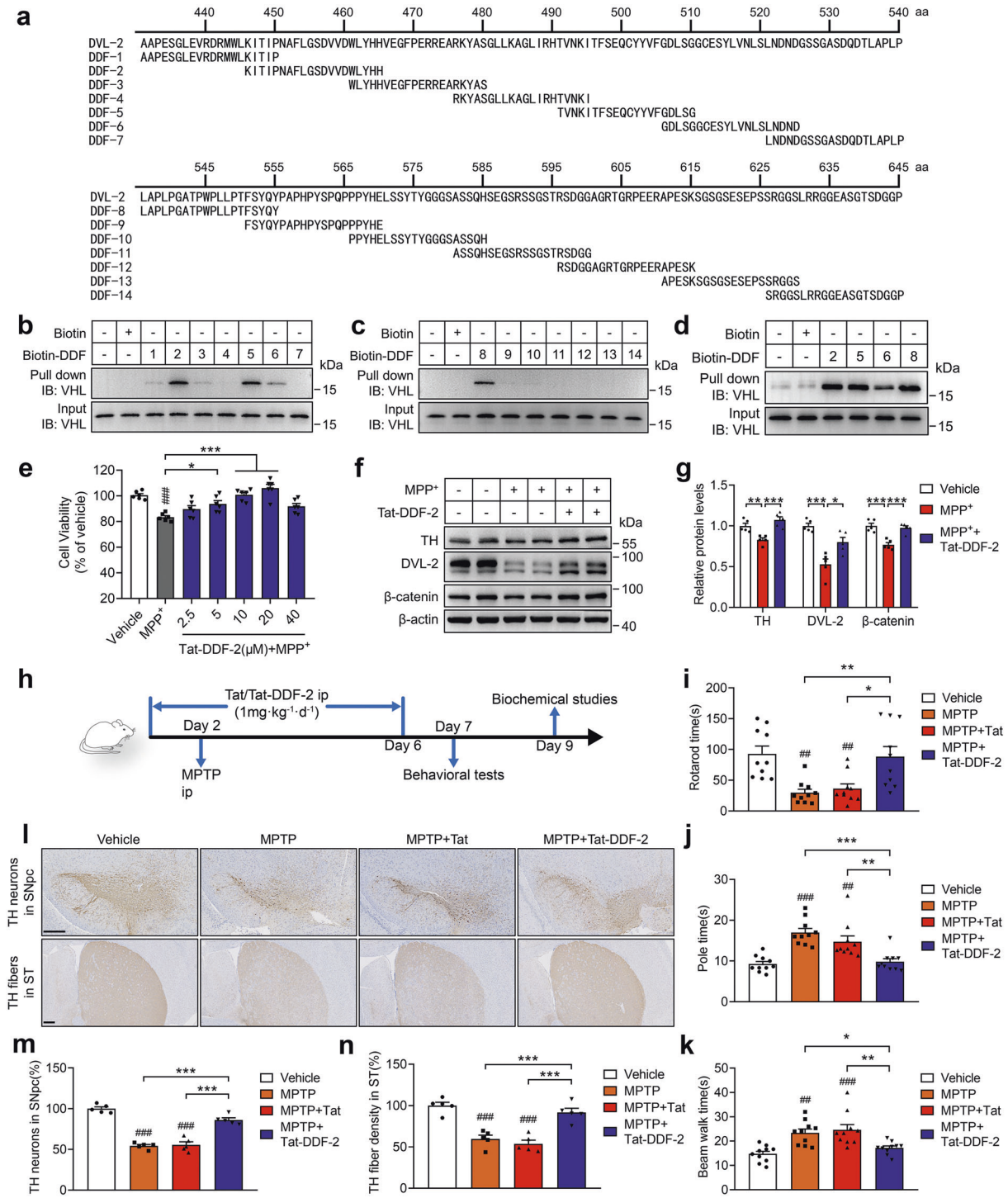

Fig. 6 Design and screening of the competing peptide targeting VHL/DVL-2 and evaluation of its protection against PD. a Design of a series of peptides based on the VHL/DVL-2 interaction. **b**–**d** Analysis of the direct interaction between DDFs and VHL using a pull-down assay. **e** Quantification of cell viability in the MPP^+-induced injury model incubated with Tat-DDF-2 (2.5, 5, 10, 20, and 40 μM) and treated with MPP^+ (150 μM). Data are the mean ± SEM; $n = 6$; statistical significance was determined by using one-way ANOVA followed by Tukey's correction. **f** Representative immunoblots of TH, DVL-2, β-catenin, and β-actin from differentiated SH-SY5Y cells incubated with Tat-DDF-2 (20 μM) and treated with MPP^+ (150 μM) for 24 h. **g** Quantification of TH, DVL-2, and β-catenin levels normalized to β-actin. Data are the mean ± SEM; $n = 5$; statistical significance was determined by using one-way ANOVA followed by Tukey's correction. **h** Procedure diagram of the animal experimental design. **i**–**k** Behavioral experiments. Data are the mean ± SEM; $n = 10$ mice for each group; statistical significance was determined by using one-way ANOVA followed by Tukey's correction. **i** Rotarod test. **j** Pole test. **k** Beam walking test. **l** Representative images from coronal sections. Scale bar, 250 μm. **m**, **n** Unbiased stereology counts of TH-positive neurons in the SNpc and quantification of TH fiber in the ST. Data are the mean ± SEM; $n = 5$; statistical significance was determined by using one-way ANOVA followed by Tukey's correction. $^{\#\#}P < 0.01$, $^{\#\#\#}P < 0.001$ vs vehicle group. $^{*}P < 0.05$, $^{**}P < 0.01$, $^{***}P < 0.001$.

elegans and mammals via the DVL-2/β-catenin axis, suggesting the potential of the VHL/DVL-2/β-catenin axis as an anti-PD therapeutic target. Genetic and pharmacological evidence in our study suggests that targeting VHL/DVL-2 is a promising strategy in the treatment of neurodegenerative disease and provides foundations for the development of DDF peptides as potential therapeutic disease-modifying agents for PD. However, several issues, such as the druggability of DDFs, still need to be further addressed. Moreover, the neuroprotective efficacy of targeting VHL/DVL-2 in other neurodegenerative diseases, including Alzheimer's disease, is also worth exploring further.

ACKNOWLEDGEMENTS

This study was supported by the National Natural Science Foundation of China (Nos. 82173728, 81872850, 82073755 and 81673435), the "Double First-Class" University Project (No. CPU2018GF08), Qing Lan Project of Jiangsu Province and PAPD (A Project Funded by the Priority Academic Program Development of Jiangsu Higher Education Institutions).

AUTHOR CONTRIBUTIONS

JS: Conceptualization, Methodology, Investigation, Writing-Original Draft, Writing-Review and Editing. QZ: Conceptualization, Methodology, Investigation, Writing-Original Draft, Writing-Review and Editing. QHY: Conceptualization, Methodology, Investigation, Writing-Original Draft, Writing-Review and Editing. YQZ: Investigation. XL: Investigation. YJC: Investigation. GXQ: Investigation. XJZ: Investigation. WBY: Conceptualization, Writing-Review and Editing, Funding acquisition, Supervision. XDG: Conceptualization, Writing-Review and Editing, Funding acquisition, Supervision. SC: Conceptualization, Writing-Review and Editing, Funding acquisition, Supervision.

ADDITIONAL INFORMATION

Supplementary information The online version contains supplementary material available at https://doi.org/10.1038/s41401-022-01014-1.

Competing interests: The authors declare no competing interests. XDG, SC, QHY, YQZ and WBY have applied for patent related to this study.

REFERENCES

1. Olsen AL, Feany MB. PARP inhibitors and Parkinson's disease. N Engl J Med. 2019;380:492–4.
2. Dorsey ER, Bloem BR. The Parkinson pandemic-a call to action. JAMA Neurol. 2018;75:9–10.
3. Hayes MT. Parkinson's disease and Parkinsonism. Am J Med. 2019;132:802–7.
4. Przedborski S. The two-century journey of Parkinson disease research. Nat Rev Neurosci. 2017;18:251–9.
5. Kalia LV, Lang AE. Parkinson disease in 2015: Evolving basic, pathological and clinical concepts in PD. Nat Rev Neurol. 2016;12:65–6.
6. Poewe W, Seppi K, Tanner CM, Halliday GM, Brundin P, Volkmann J, et al. Parkinson disease. Nat Rev Dis Prim. 2017;3:17013.
7. Faure P, Tolu S, Valverde S, Naude J. Role of nicotinic acetylcholine receptors in regulating dopamine neuron activity. Neuroscience. 2014;282:86–100.
8. Patel JC, Rossignol E, Rice ME, Machold RP. Opposing regulation of dopaminergic activity and exploratory motor behavior by forebrain and brainstem cholinergic circuits. Nat Commun. 2012;3:1172.
9. Schultz W. Multiple dopamine functions at different time courses. Annu Rev Neurosci. 2007;30:259–88.
10. Verharen JPH, de Jong JW, Lammel S. Dopaminergic control over the tripartite synapse. Neuron. 2020;105:954–6.
11. Krashia P, Cordella A, Nobili A, La Barbera L, Federici M, Leuti A, et al. Blunting neuroinflammation with resolvin D1 prevents early pathology in a rat model of Parkinson's disease. Nat Commun. 2019;10:3945.
12. Bankapalli K, Vishwanathan V, Susarla G, Sunayana N, Saladi S, Peethambaram D, et al. Redox-dependent regulation of mitochondrial dynamics by DJ-1 paralogs in Saccharomyces cerevisiae. Redox Biol. 2020;32:101451.
13. Langston JW. The MPTP story. J Parkinsons Dis. 2017;7:S11–9.
14. Guo RY, Zong S, Wu M, Gu JK, Yang MJ. Architecture of human mitochondrial respiratory megacomplex $I_2III_2IV_2$. Cell. 2017;170:1247–57.
15. Pitkanen S, Robinson BH. Mitochondrial complex I deficiency leads to increased production of superoxide radicals and induction of superoxide dismutase. J Clin Invest. 1996;98:345–51.
16. Giachin G, Bouverot R, Acajjaoui S, Pantalone S, Soler-López M. Dynamics of human mitochondrial complex I assembly: implications for neurodegenerative diseases. Front Mol Biosci. 2016;3:43.
17. Chen S, Luo S, Zhang Z, Ma DK. VHL-1 inactivation and mitochondrial antioxidants rescue *C. elegans* dopaminergic neurodegeneration. Protein Cell. 2019;10:610–4.
18. Ferrari M, Jain IH, Goldberger O, Rezoagli E, Thoonen R, Cheng KH, et al. Hypoxia treatment reverses neurodegenerative disease in a mouse model of Leigh syndrome. Proc Natl Acad Sci USA. 2017;114:E4241–50.
19. Wu Y, Jiang ZS, Li ZH, Gu J, You QD, Zhang XJ. Click chemistry-based discovery of [3-Hydroxy-5-(1 H-1,2,3-triazol-4-yl)picolinoyl]glycines as orally active hypoxia-inducing factor prolyl hydroxylase inhibitors with favorable safety profiles for the treatment of anemia. J Med Chem. 2018;61:5332–49.
20. Chen S, Liu AR, An FM, Yao WB, Gao XD. Amelioration of neurodegenerative changes in cellular and rat models of diabetes-related Alzheimer's disease by exendin-4. Age. 2012;34:1211–24.
21. Kamath RS, Martinez-Campos M, Zipperlen P, Fraser AG, Ahringer J. Effectiveness of specific RNA-mediated interference through ingested double-stranded RNA in *Caenorhabditis elegans*. Genome Biol. 2001;2:Research0002.1–10.
22. Xu DP, Duan HW, Zhang ZJ, Cui W, Wang L, Sun YW, et al. The novel tetramethylpyrazine bis-nitrone (TN-2) protects against MPTP/MPP^+-induced neurotoxicity via inhibition of mitochondrial-dependent apoptosis. J Neuroimmune Pharmacol. 2014;9:245–58.
23. Frost J, Galdeano C, Soares P, Gadd MS, Grzes KM, Ellis L, et al. Potent and selective chemical probe of hypoxic signalling downstream of HIF-α hydroxylation via VHL inhibition. Nat Commun. 2016;7:13312.
24. Besarab A, Chernyavskaya E, Motylev I, Shutov E, Kumbar LM, Gurevich K, et al. Roxadustat (FG-4592): correction of anemia in incident dialysis patients. J Am Soc Nephrol. 2016;27:1225–33.
25. Koh MY, Spivak-Kroizman TR, Powis G. Inhibiting the hypoxia response for cancer therapy: the new kid on the block. Clin Cancer Res. 2009;15:5945–6.
26. Zhang J, Wu T, Simon J, Takada M, Saito R, Fan C, et al. VHL substrate transcription factor ZHX2 as an oncogenic driver in clear cell renal cell carcinoma. Science. 2018;361:290–5.
27. Corn PG, McDonald ER 3rd, Herman JG, El-Deiry WS. Tat-binding protein-1, a component of the 26S proteasome, contributes to the E3 ubiquitin ligase function of the von Hippel-Lindau protein. Nat Genet. 2003;35:229–37.
28. Ma BY, Liu BF, Cao WP, Gao C, Qi Z, Ning YH, et al. The wnt signaling antagonist Dapper1 accelerates Dishevelled2 degradation via promoting its ubiquitination and aggregate-induced autophagy. J Biol Chem. 2015;290:12346–54.
29. Metcalfe C, Ibrahim AE, Graeb M, de la Roche M, Schwarz-Romond T, Fiedler M, et al. Dvl2 promotes intestinal length and neoplasia in the Apc^{Min} mouse model for colorectal cancer. Cancer Res. 2010;70:6629–38.
30. Huang SM, Mishina YM, Liu SM, Cheung A, Stegmeier F, Michaud GA, et al. Tankyrase inhibition stabilizes axin and antagonizes Wnt signalling. Nature. 2009;461:614–20.
31. Armstrong MJ, Okun MS. Time for a new image of Parkinson disease. JAMA Neurol. 2020;77:1345–6.
32. Arun S, Liu L, Donmez G. Mitochondrial biology and neurological diseases. Curr Neuropharmacol. 2016;14:143–54.
33. Hsieh CH, Shaltouki A, Gonzalez AE, Bettencourt da Cruz A, Burbulla LF, St Lawrence E, et al. Functional impairment in miro degradation and mitophagy is a shared feature in familial and sporadic Parkinson's disease. Cell Stem Cell. 2016;19:709–24.
34. Schapira AH, Cooper JM, Dexter D, Jenner P, Clark JB, Marsden CD. Mitochondrial complex I deficiency in Parkinson's disease. Lancet. 1989;1:1269.
35. Anglade P, Vyas S, Javoy-Agid F, Herrero MT, Michel PP, Marquez J, et al. Apoptosis and autophagy in nigral neurons of patients with Parkinson's disease. Histol Histopathol. 1997;12:25–31.
36. Wang YQ, Chen C, Huang WL, Huang MX, Wang JH, Chen XC, et al. Beneficial effects of PGC-1α in the substantia nigra of a mouse model of MPTP-induced dopaminergic neurotoxicity. Aging. 2019;11:8937–50.
37. Triepels RH, van den Heuvel LP, Loeffen JL, Buskens CA, Smeets RJ, Rubio Gozalbo ME, et al. Leigh syndrome associated with a mutation in the NDUFS7 (PSST) nuclear encoded subunit of complex I. Ann Neurol. 1999;45:787–90.
38. Fiedorczuk K, Sazanov LA. Mammalian mitochondrial complex I structure and disease-causing mutations. Trends Cell Biol. 2018;28:835–67.
39. Zhu YY, Zhao YX, Zou L, Zhang DF, Aki D, Liu YC. The E3 ligase VHL promotes follicular helper T cell differentiation via glycolytic-epigenetic control. J Exp Med. 2019;216:1664–81.

40. Cargill K, Hemker SL, Clugston A, Murali A, Mukherjee E, Liu J, et al. Von Hippel-Lindau acts as a metabolic switch controlling nephron progenitor differentiation. J Am Soc Nephrol. 2019;30:1192–205.
41. Nguyen-Tran HH, Nguyen TN, Chen CY, Hsu T. Endothelial reprogramming stimulated by oncostatin M promotes inflammation and tumorigenesis in VHL-deficient kidney tissue. Cancer Res. 2021;81:5060–73.
42. Jaakkola P, Mole DR, Tian YM, Wilson MI, Gielbert J, Gaskell SJ, et al. Targeting of HIF-alpha to the von Hippel-Lindau ubiquitylation complex by O_2-regulated prolyl hydroxylation. Science. 2001;292:468–72.
43. Gao C, Cao WP, Bao L, Zuo W, Xie GM, Cai TT, et al. Autophagy negatively regulates Wnt signalling by promoting Dishevelled degradation. Nat Cell Biol. 2010;12:781–90.